Available online at www.sciencedirect.com
ScienceDirect
Journal of the European Ceramic Society 31 (2011) 2255–2265
www.elsevier.com/locate/jeurceramsoc

Oxidation behaviour of nano-sized SiC particulate reinforced Alon composites

X.J. Zhao [a,b], D.L. Chen [b,*], H.Q. Ru [a,**], N. Zhang [c], B. Liang [c]

[a] Department of Materials Science and Engineering, School of Materials and Metallurgy, Northeastern University, Shenyang, Liaoning 110004, China
[b] Department of Mechanical and Industrial Engineering, Ryerson University, Toronto, Ontario M5B 2K3, Canada
[c] Key Laboratory of Advanced Materials Manufacturing Technology of Liaoning Province, Shenyang University, Shenyang, Liaoning 110044, China

Received 7 May 2011; accepted 19 May 2011
Available online 1 July 2011

Abstract

Silicon carbide (SiC)–aluminium oxynitride (Alon) ceramic composites exhibited improved mechanical properties, but the high temperature oxidation behaviour was unknown. The aim of this investigation was to identify oxidation characteristics and kinetics of 8 wt% SiC–Alon composites over a temperature range between 700 °C and 1200 °C in air. The Alon matrix and SiC particles near the surface were oxidized to form Al_2O_3 and SiO_2, respectively. The starting oxidation temperature of Alon was observed to be about 1000 °C. While the addition of nano-sized SiC particles resulted in a reduced starting oxidation temperature due to the large cumulative surface area and high total surface energy, the oxidation resistance at higher temperatures of 1100 °C and 1200 °C was remarkably enhanced. The oxidation kinetics changed from a linear weight gain for pure Alon into a logarithmic weight gain for the composites due to the formation of a dense protective oxidation layer arising from the presence of SiO_2.

Keywords: Alon; SiC; Composites; Hot pressing; Corrosion; Oxidation

1. Introduction

Spinel aluminium oxynitride (Alon) is a solid solution of Al_2O_3 and AlN.[1,2] Due to its excellent chemical and mechanical properties such as high rigidity, good chemical stability and good wear resistance against steel, Alon has become a potential ceramic material for high-performance structural and advanced refractory applications.[3,4] Oxidation resistance is an important property of materials for high-temperature applications. At present oxides are widely used as refractory materials. However, varying working conditions and severe environments require the development of new refractories. In general, densified oxides have excellent corrosion resistance, but their thermal shock resistance is poor,[5] e.g., alumina (Al_2O_3) being such a type.[6] On the other hand, silicon nitride and silicon carbide possess good mechanical properties but exhibit rather poor oxidation resistance. These ceramic materials are in a major competition with the newer type of Alon and Sialon systems developed in the early 1970s.[6] For example, Goeuriot et al.[7] reported that the performance of Alon at high temperatures, such as the corrosion resistance against molten steel, is superior to that of alumina.

A number of researchers[1,8–12] have studied the oxidation behaviour of Alon and SiC. However, the reported results of Alon ceramic are not always consistent with each other, and the oxidation mechanism is still far from being completely understood. Corbin[1] reported that the oxidation of Alon produced a protective oxide layer up to 1200 °C. But some other authors did not observe such a protective layer.[13] Lefort et al.[11] reported that the oxidation could not be observed below 1200 °C and a maximum weight gain was reached at about 1550 °C. However, Wang et al.[8] found that Alon could be oxidized at a temperature of about 1000 °C in air and the oxidation product formed a protective layer which offered resistance to further oxidation below 1200 °C. Goursat et al.[12] observed that the oxidation started even at about 650 °C and reached a maximum weight gain at 1150 °C. When heating was beyond this temperature a weight loss occurred. It can be seen that there are still some inconsistent results on the oxidation of Alon below 1200 °C.

The oxidation behaviour of Alon ceramic at high temperatures could be improved by adding other particles, e.g., TiN[14]

* Corresponding author. Tel.: +1 416 979 5000x6487; fax: +1 416 979 5265.
** Corresponding author. Tel.: +86 024 83680248; fax: +86 024 83680248.
E-mail addresses: dchen@ryerson.ca (D.L. Chen), ruhq@smm.neu.edu.cn (H.Q. Ru).

0955-2219/$ – see front matter © 2011 Elsevier Ltd. All rights reserved.
doi:10.1016/j.jeurceramsoc.2011.05.049

and $SiAl_7O_2N_7$.[15] SiC particles were normally added into Alon ceramic to improve the mechanical properties and enhance the resistance to damage arising from thermal quench due to good thermal conductivity of SiC,[16] and form a solid solution owing to the similarity in the crystal structure of γ-Alon and β-SiC.[17] To the authors' knowledge, there is no report regarding the oxidation of SiC–Alon composites in the literature. It is unclear if the oxidation of SiC–Alon ceramic composites can occur below 1200 °C, to what extent the SiC addition can improve the oxidation resistance of Alon ceramic, and if mullite can occur when the SiC–Alon composites become oxidized. It should be noted that mullite, with a chemical composition ranging from $3Al_2O_3$–$2SiO_2$ to approximately $2Al_2O_3$–SiO_2,[18] is a stable crystalline phase in the aluminosilicate system under normal atmospheric pressure at room through elevated temperatures.[19] The aim of the present study was, therefore, to evaluate the oxidation characteristics and kinetics of SiC–Alon composites below 1200 °C in air and identify the underlying mechanisms of oxide formation.

2. Materials and methods

In the present study the raw materials were nano-sized Al_2O_3 (40–100 nm, Nanjing Emperor Nano Material Co., Ltd., China, 99.5%), AlN (30–100 nm, Shenzhen Honesty Nano-Tech Co., Ltd., China, 99%), SiC (40–90 nm, Nanjing Emperor Nano Material Co., Ltd., China, 99.5%) powders and a small amount micro-sized Al powders (4–8 μm, Gaizhou City Metal Powder Factory, China, 99.63%). A mixture with a weight ratio of 81:18:1 for Al_2O_3:AlN:Al was selected to synthesize monolithic Alon. Then 8 wt% nano-sized SiC particles were added to the mixture. The thoroughly mixed powders were attrition milled for 24 h using ethanol as a milling medium, then dried at 80 °C. The dry mixed SiC–Alon powders were crushed using mortar and then sieved through an 180 μm mesh. The mixed powders as well as pure Alon powders were put in a graphite die and sintered at 1850 °C under a pressure of 25 MPa for 40 min in nitrogen atmosphere using a heating rate of 10 °C/min below 1400 °C and then 5 °C/min up to the selected sintering temperature. Finally the sintered SiC–Alon composites were furnace-cooled down to room temperature.

To examine the oxidation characteristics of Alon and SiC–Alon composites, the weight change of the specimens was measured. The specimens with a dimension of 5 mm × 5 mm × 30 mm were cut and machined from the hot-pressed samples. The oxidation tests were carried out in an electric furnace in air environment with a heating rate of 5 °C/min at a constant temperature ranging between 700 °C and 1200 °C for 40 h. The weight gains resulting from the oxidation were measured by an electric balance with a resolution of 0.1 mg. Within the first 8 h the weight gain was measured every hour, and then it was measured every 8 h. To identify the oxidation behaviour of Alon and SiC–Alon composites differential scanning calorimetry (DSC) tests were performed in an air atmosphere using a heating rate of 10 °C/min from 200 °C to 1500 °C.

The microstructures of both powders and oxidation products were examined using a scanning electron microscope (SEM). The elemental concentration profile of the microstructure was determined using energy dispersive X-ray spectroscopy (EDS). To determine the thickness of the oxidation layers from the cross section, two samples were clamped together using an aluminium holder, and then ground and polished to a surface finish down to 1 μm diamond paste in the same way so as to protect the oxidation layer. To achieve a better resolution on the SEM images, the specimens were sputter-coated with a thin film of gold.

The phase and crystallinity were analyzed via X-ray diffraction (XRD) using CuK_α radiation at 45 kV and 40 mA. The diffraction angle (2θ) at which the X-rays hit the sample varied from 10° to 90° with a step size of 0.05° and 1 s in each step. After the peaks corresponding to (1 1 1) of SiO_2 and (0 0 6) of SiC had been identified, a much lower (i.e., 40 times slower) scan rate at a step size of 0.01° and duration time of 8 s in each step was used with a diffraction angle range varying from 34.6° to 36.3° for an more detailed analysis.

3. Results

3.1. Raw powders and synthesized Alon analysis

Fig. 1 shows the SEM micrographs of the prepared Alon powders and SiC powders. It is seen from Fig. 1(a) that the prepared Alon powders had an average size of about 5 μm and a spinel-type structure as reported by Corbin.[1] Fig. 1(b) shows that most of SiC particles were nano-sized (<100 nm), but there also appeared a conglomeration because it was normally difficult to disperse nano-sized particles on a copper plate after ultrasonic vibration for SEM imaging.

Fig. 2 shows the XRD patterns of pure Alon and 8 wt% SiC–Alon composites prior to oxidation. In both Fig. 2(a) and (b), the atomic ratio of Alon phase allowed the determination of the γ-Alon formula as $Al_{2.81}O_{3.56}N_{0.44}$, which was the same as that reported by Goeuriot et al.[7] It is seen from Fig. 2(a) that the obtained Alon exhibited a typical XRD pattern of Alon without decomposition (i.e., no other by-products present). It should be pointed out that there was, however, a little bit residual Al_2O_3 presented in the pure Alon or SiC–Alon composites. This was due to the fact that the Alon powders were synthesized from Al_2O_3 and AlN in a nitrogen atmosphere. The synthesized Alon powders by solid reaction method normally contained a little remaining Al_2O_3 or AlN.[20,21] Fig. 2(b) shows the XRD results of 8 wt% SiC–Alon composites fabricated using hot pressing technique. The spectra revealed that the main phases were γ-Alon, SiC and a small amount of Al_2O_3 as well. Again, no other new phases or impurities could be identified in the pattern. Thus the XRD results shown in Fig. 2 suggested that the structure of Alon and SiC–Alon composites obtained in the present study was thermally stable enough after hot-press sintering at 1850 °C in a nitrogen atmosphere.

3.2. DSC analysis and microstructure

Fig. 3 shows the curves of DSC and thermogravimetry (TG) for 8 wt% SiC–Alon composite sample. It is seen that there

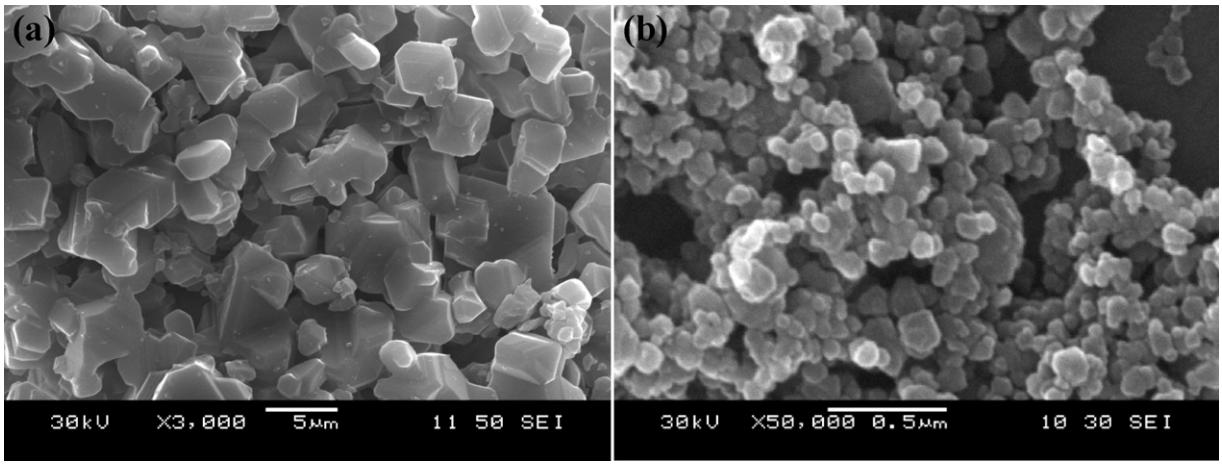

Fig. 1. SEM images of raw powders for the (a) micro-sized Alon powders and (b) nano-sized SiC powders.

was no decalescence (or absorption of heat) in the range of 200–1350 °C, but there was a significant weight gain after the temperature reached about 700 °C from the TG curve in Fig. 3. This would be attributed to the occurrence of oxidation starting at about 700 °C. When the temperature reached about 1370 °C, there was an obvious decalescence peak on the DSC curve in Fig. 3. This was likely due to a solid-state transformation occurred from the metastable γ-Al_2O_3 to α-Al_2O_3. As Wang et al.[8] reported, the product formed at lower temperatures was metastable γ-Al_2O_3, being a protective layer which offered resistance to further oxidation. The γ-Al_2O_3 was then transformed to α-Al_2O_3 since the product was clearly identified to be α-Al_2O_3 when the temperature was above 1370 °C. Since the weight gain seen from the TG curve in Fig. 3 started from about 700 °C, indicating the onset of oxidation, the subsequent oxidation tests were carried out from 700 °C to 1200 °C.

To demonstrate the microstructure (grain size and SiC particles), SEM micrographs of fracture surfaces of the sintered pure Alon and 8 wt% SiC–Alon composites without oxidation after three-point bending tests are shown in Fig. 4. The Alon matrix grains and tiny SiC particles could be seen from the fractographs, with some SiC particles homogeneously distributed in the Alon matrix and some located at grain boundaries or triple junctions of Alon grains (as indicated by arrows in Fig. 4(b)), but they still remained to be nano-sized after sintering at 1850 °C. It is of interest to note that the addition of nano-sized SiC particles effectively restricted the growth of grains and led to a refined Alon matrix grain size, as compared Fig. 4(a) with (b) taken at the same magnification of 5000×. This was due to the pinning role

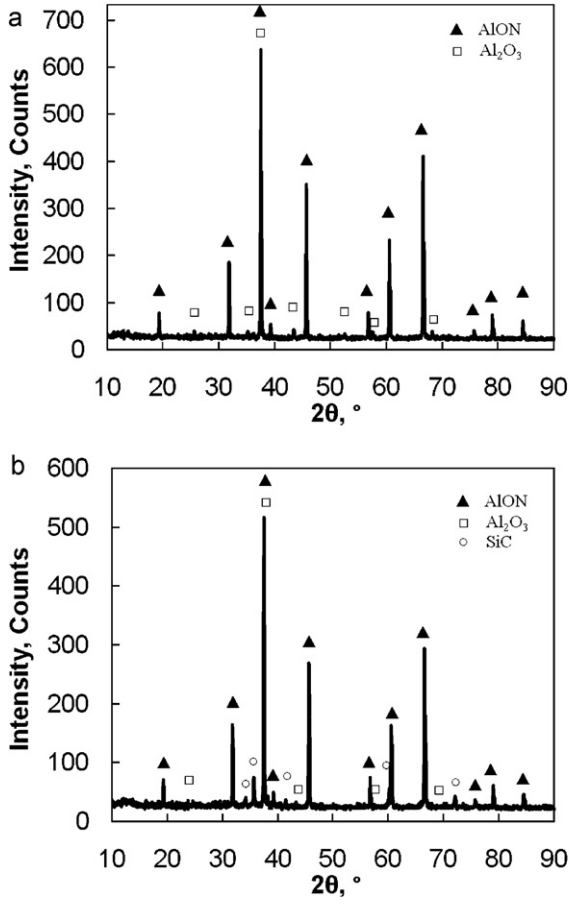

Fig. 2. XRD patterns of (a) pure Alon and (b) 8 wt% SiC–Alon composites sintered in a nitrogen atmosphere at 1850 °C.

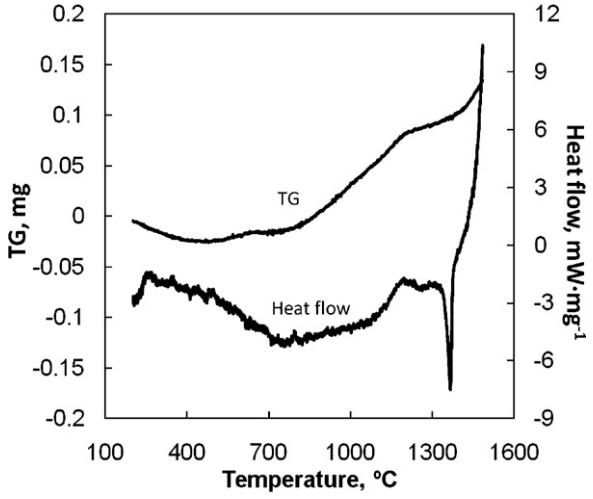

Fig. 3. Curves of DSC and TG for 8 wt% SiC–Alon composite sample.

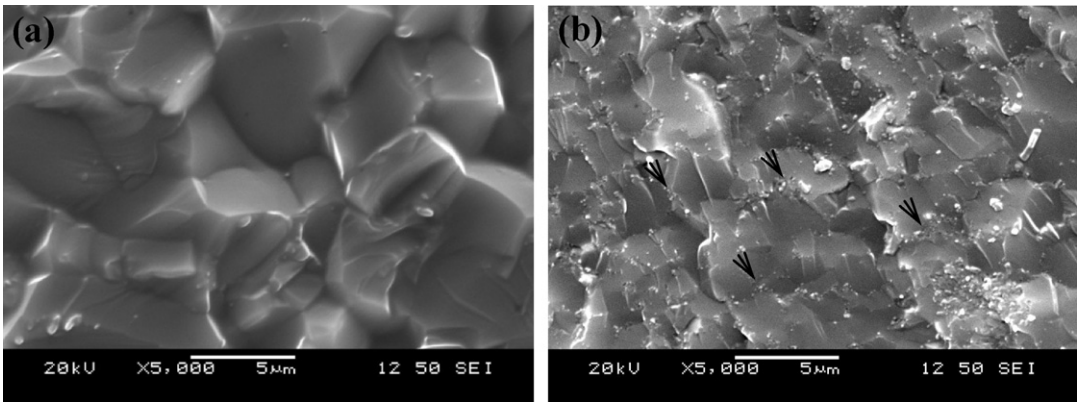

Fig. 4. SEM images of fracture surfaces after three point bending tests before oxidation experiments: (a) pure Alon, and (b) 8 wt% SiC–Alon.

(Zener pinning pressure) of the nano-sized SiC particles positioned at grain boundaries or triple junctions of Alon, since the pinning by dispersed particles was one of the well-recognized processes that reduced the driving force for grain growth.[22,23] Such nanocomposites would exhibit a strong resistance to crack initiation during plastic deformation as reported recently by Guo and Todd.[24]

3.3. Weight change during oxidation

Fig. 5 shows the weight changes of the pure Alon and SiC–Alon specimens oxidized at various temperatures with time. It can be seen that when the oxidation occurred, the weight all increased with increasing oxidation time. As seen from Fig. 5(a), the weight of Alon specimen hardly changed before 900 °C. But when the temperature was higher than 1000 °C, the specimen began to be oxidized, and the weight gain exhibited a linear-like increase. Similar linear kinetics of Alon oxidation was reported by Goeuriot et al.[7] This was related to the microstructure of the oxidation layer to be shown later. Furthermore, the oxidation rate (i.e., the slope of the curve of weight gain vs. time) increased with increasing temperature. On the other hand, it can be seen from Fig. 5(b) that almost all the curves had typically a high weight increase in the initial stage but it slowed down in the later stage, following basically a logarithmic relationship. This suggested that the nano-sized SiC particles added to the Alon matrix played a key role in changing the kinetic behaviour of oxidation in SiC–Alon composites. When the temperature was 700 °C, the weight of SiC–Alon increased slightly with increasing oxidation time. Before the temperature reached up to 1000 °C, the oxidation rate increased with increasing temperature. However, when the temperature further increased to 1100 °C and 1200 °C, the rate of weight gain considerably decreased especially at 1100 °C. A detailed explanation will be presented in Section 4.

3.4. Microstructural change during oxidation

Fig. 6 shows some typical SEM micrographs of the surfaces of the specimens after oxidation at various temperatures, where different morphologies appeared on the sample surfaces. The oxidation products of both Alon ceramic and SiC–Alon composites observed at 900 °C (Fig. 6(a) and (b)) basically lay in the initial oxidation stage, with similar microstructural morphology (tiny needle-like features). With increasing oxidation temperature to 1100 °C (Fig. 6(c) and (d)), the needle-like oxidation products became larger. At 1200 °C the morphology of the oxidation layer significantly changed and the needle-like oxidation products were no longer present (Fig. 6(e) and (f)). Compared Fig. 6(e) with (f), an obvious denser oxidation layer was seen

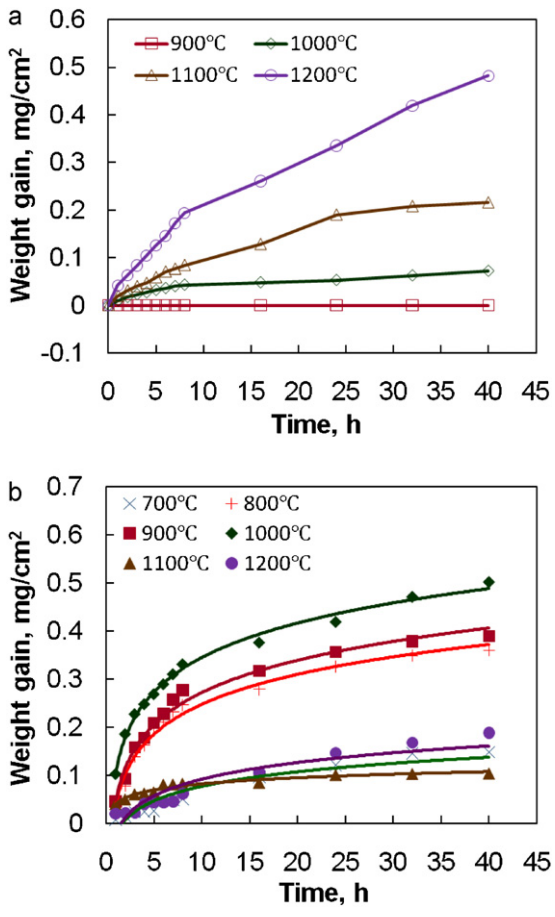

Fig. 5. Weight changes as a function of oxidation time for (a) pure Alon and (b) 8 wt% SiC–Alon composites at various temperatures.

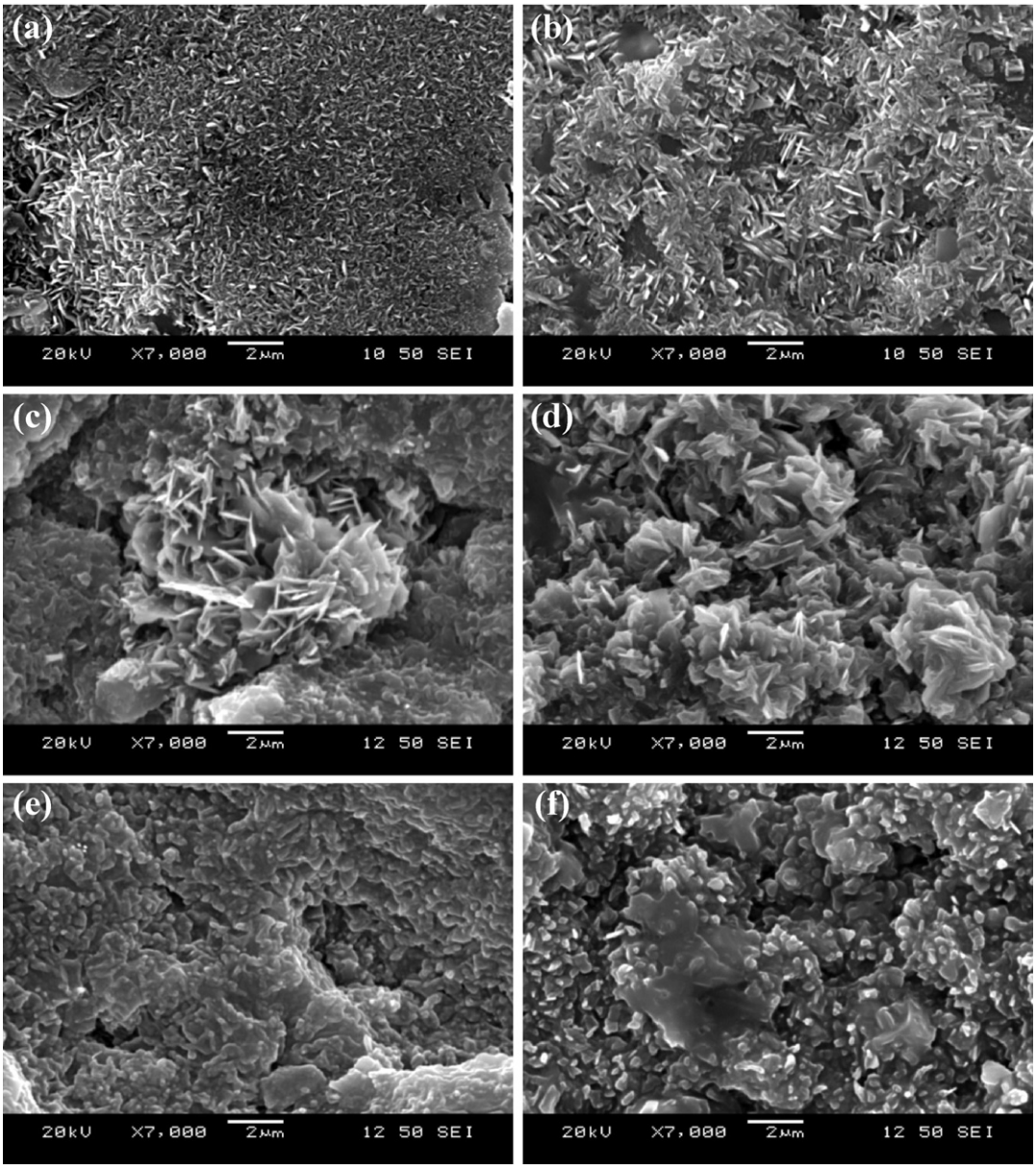

Fig. 6. SEM micrographs of specimen surfaces after oxidation in air for 40 h: (a) pure Alon at 900 °C; (b) SiC–Alon composites at 900 °C; (c) pure Alon at 1100 °C; (d) SiC–Alon composites at 1100 °C; (e) pure Alon at 1200 °C; and (f) SiC–Alon at 1200 °C.

to form in the SiC–Alon composites, mainly resulting from the formation of SiO_2. The details will be presented in Section 4.

Fig. 7 shows an EDS line scan indicating the profile of oxygen element across the boundary between the oxidation layer and Alon matrix along the cross section of the sample oxidized at 1200 °C in air for 40 h. It is clear that the oxygen was considerably higher in the layer near the specimen surface. It should be noted that the white surface layer was partially gone during grinding and polishing even though two samples were attached side by side to have a better protection of the surface layer. This was mainly due to the looseness of the oxidation products, as shown in Fig. 6. Beyond this layer in the inner part of the sample, the oxygen decreased only slightly. That is, an abrupt change in the oxygen composition from the EDS line scan can be easily identified. Based on the information of both the oxygen composition change and the white surface layer reflecting its looseness, the white surface layer was considered as the oxide layer in the present study, and the thickness of the surface oxide layer was assessed accordingly.

Fig. 8 shows the thickness changes of the surface oxide layer in the Alon and SiC–Alon composites that were oxidized at various temperatures for 40 h. It is seen that the Alon and SiC–Alon composites did not exhibit an obvious change up to 700 °C, with an oxide layer thickness of about 5–10 μm in the two specimens oxidized at 700 °C in air for 40 h (Fig. 8(a) and (b)). When the specimens were oxidized at 900 °C, the Alon sample still had no significant change (Fig. 8(c)), but an oxide layer of about 90 μm in the SiC–Alon specimen occurred (Fig. 8(d)). However,

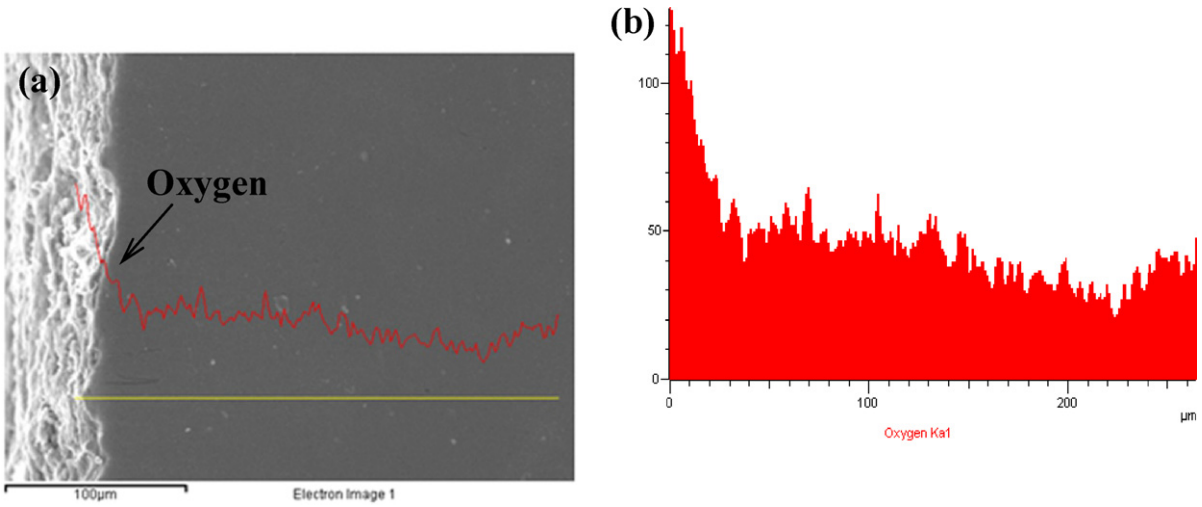

Fig. 7. EDS line scan showing the distribution of oxygen along the cross section of a polished Alon sample that was oxidized at 1200 °C in air for 40 h, (a) overall view and (b) magnified view of the compositional variation.

at 1200 °C the Alon specimen had an oxidation layer of about 180 μm (Fig. 8(e)), whereas the oxidation layer of SiC–Alon specimen became thinner (about 70 μm). These observations corresponded well to the results of weight gain shown in Fig. 5. One can also see from Fig. 8 that the non-oxidized samples (at the lower portion of the images) were pretty dense which matched with the relative density of more than 97% measured.

3.5. Phase change during oxidation

Fig. 9 shows the XRD pattern of the oxidized Alon and SiC–Alon composites at different temperatures. It is seen that with increasing oxidation temperature, the contents of oxidation products as Al_2O_3 and SiO_2 increased. Furthermore, according to the position and intensity of the peaks from the XRD spectrum, it can be identified that there were mainly α-Al_2O_3, which had a rhombohedral crystal structure and little γ-Al_2O_3, which belonged to the cubic crystal structure. Compared the product of Al_2O_3 between Fig. 9(a) and (b), at a temperature of 900 °C the XRD pattern was similar in Alon and SiC–Alon composites. But at 1100 °C or 1200 °C, the intensity of Al_2O_3 peaks was seen to be significantly higher than that of SiC–Alon composites oxidized at the same temperature, corresponding well to the results shown in Figs. 5 and 8. However, it was difficult to identify the change of SiC and SiO_2 from Fig. 9(b) since the intensity of the SiC and SiO_2 peaks was relatively weak due to the faster scan. To examine the change of SiC and SiO_2 peaks in the SiC–Alon composites with the oxidation temperature, a much (or 40 times) slower scan with a step size of 0.01° and duration of 8 s in each step was performed from 34.6° to 36.3°, within which the strongest peaks of both SiC and SiO_2 [i.e. (1 1 1) peak of SiO_2 and (0 0 6) peak of SiC] were included. The obtained spectra are shown in Fig. 10. It is clear that the higher the oxidation temperature, the higher the intensity of SiO_2 peak in the SiC–Alon composites. In other words, the intensity of SiO_2 peak increased and, meanwhile, the intensity of SiC peak slightly decreased as the oxidation temperature increased.

4. Discussion

In the present study, denser Alon and SiC–Alon ceramic composites with a relative density of 97% have been successfully fabricated. While the starting oxidation temperature in the SiC–Alon composites decreased to about 700 °C, the addition of nano-sized SiC particles considerably improved the oxidation resistance of Alon ceramic when the temperature was above 1100 °C (Fig. 5(b)). The presence of SiO_2 at the high temperatures led to the formation of a dense oxidation layer on the specimen surface, which can protect the material to further oxidation (Fig. 6(f)).

Initially the Alon samples were dark and the SiC–Alon composites were gray by naked eyes. After the oxidation tests, the sample color visibly changed. At the lower oxidation temperatures (below 1000 °C) no or little sample color change occurred. However, at the higher temperatures (1100 °C and 1200 °C) the surface of Alon samples became whitened and the surface of SiC–Alon composites became darkened. Similar color changes were also observed during oxidation in the mullite–SiC composites.[25] The oxidation could generally be characterized by five steps: (1) contact of oxygen in the atmosphere to the sample, (2) inward diffusion of oxygen through the oxidation layer, (3) oxidation reaction at the interface between the matrix and the oxidation layer, (4) outward diffusion of the gaseous product through the oxidation layer, and (5) outward flow of product gases away from the surface.[26]

4.1. Oxidation behaviour of Alon ceramic

As seen from Fig. 5(a), the Alon ceramic could only be oxidized in air at a temperature higher than 1000 °C. This was in agreement with the result reported by Wang et al.[8] The weight gain of Alon ceramic shown in Fig. 5 could be caused by the following reaction,[1,7]

$$4Al_{2.81}O_{3.56}N_{0.44} + 1.31O_2 \rightarrow 5.62Al_2O_3 + 0.88N_2\uparrow, \quad (1)$$

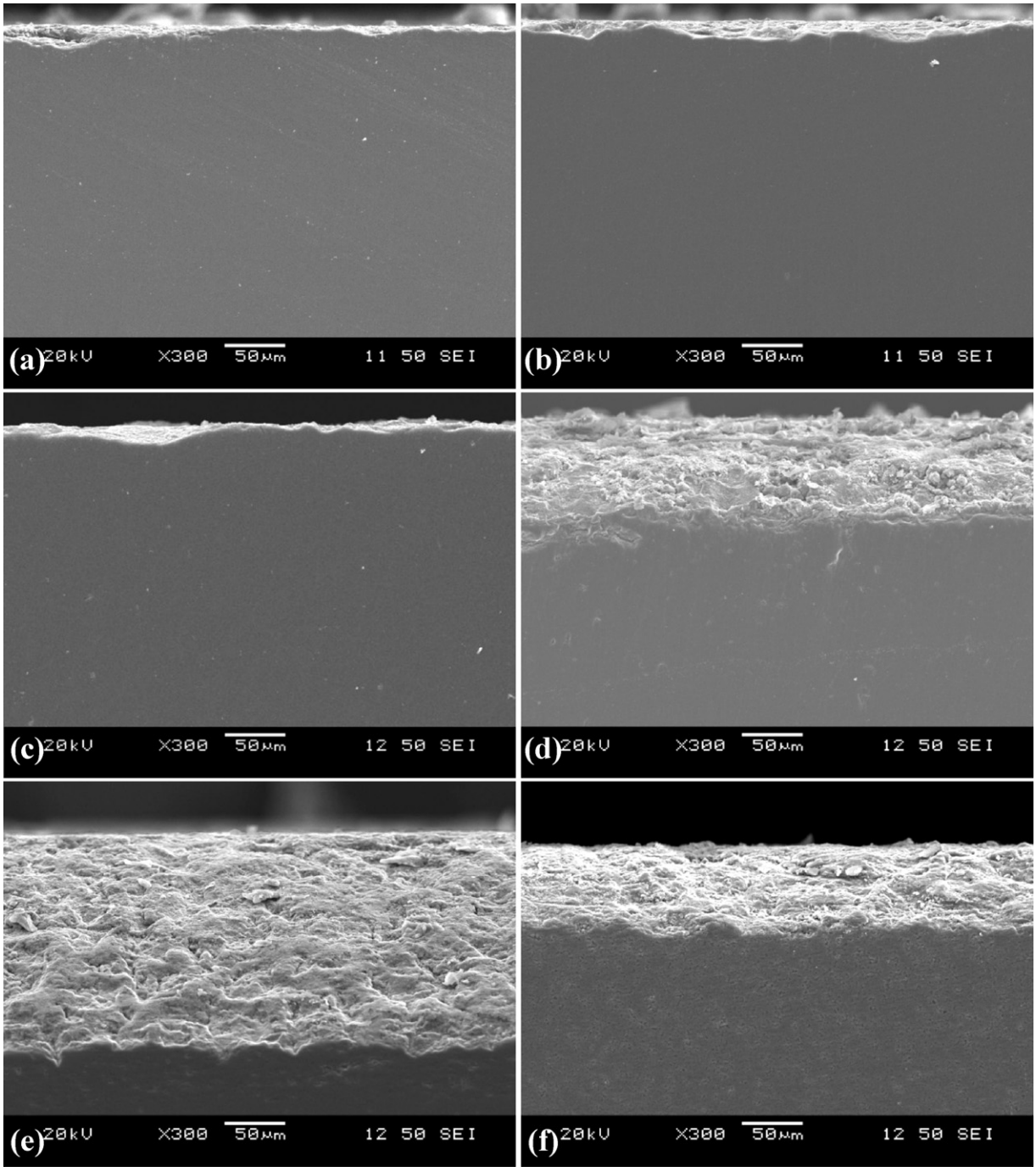

Fig. 8. SEM micrographs of the cross section of the polished samples after oxidation in air for 40 h for (a) pure Alon at 700 °C, (b) SiC–Alon at 700 °C, (c) pure Alon at 900 °C, (d) SiC–Alon at 900 °C, (e) pure Alon at 1200 °C and (f) SiC–Alon at 1200 °C.

since the molecular weight of oxygen is about 14.2% higher than that of nitrogen. This reaction could be corroborated by the presence of some nitrogen trapped in the spinel structure when the oxidation temperature was less than 1200 °C.[7] While no weight change was seen at an oxidation temperature of 900 °C (Fig. 5(a)), there was still a very thin layer of oxide lying in the initial stage on the surface (Figs. 6(a) and 8(c)). This suggested that the weight gain contributed by this very thin layer of oxide at 900 °C could be negligible. Indeed, the weight gain in the oxidation of pure Alon ceramic was not so sensitive since it was only about 3.12% per reaction based on Eq. (1). Furthermore, the formation of Al_2O_3 given in Eq. (1) could be directly verified by the XRD pattern (Fig. 9(a)) where the oxidation product in the pure Alon was identified to be Al_2O_3 only.

The oxidation products formed at high temperatures exhibited different microstructural morphologies, as shown in Fig. 6. For example, the oxidation products at 1200 °C might experience the initial needle-like morphology (Fig. 6(a) and (b)) and the subsequent growth of the needle-like crystals (Fig. 6(c) and (d)). Such needle-like crystals were also observed in the initial

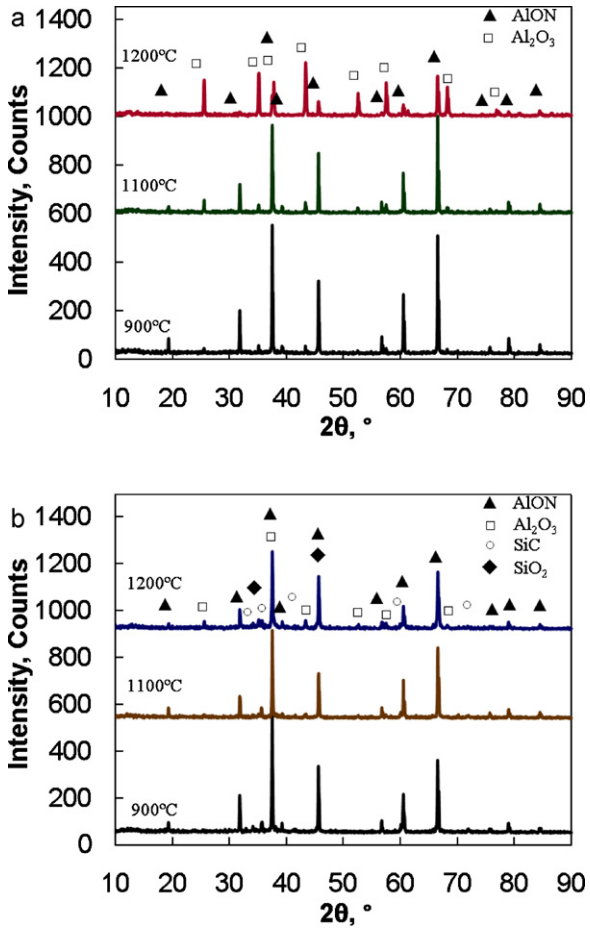

Fig. 9. XRD patterns of (a) pure Alon and (b) 8 wt% SiC–Alon composites oxidized in air for 40 h at various temperatures.

stage of oxidation in other ceramic materials.[27,28] With increasing oxidation time the oxidation product could become flake-like crystals due to the fact that the driving force was strong enough for oxidation products to grow up. At last, the oxide scale on the surface formed layer-like crystals, which could protect the matrix from further oxidation depending on the denseness or tightness.

4.2. Oxidation behaviour of SiC–Alon composites

As reported in,[29,30] the addition of SiC particles has been proven to improve the mechanical properties and oxidation resistance at high temperatures in other ceramic materials such as zirconium diboride (ZrB_2). As mentioned above, the currently added nano-sized SiC particles also played an important role in changing the oxidation characteristics and kinetics of Alon ceramic from linear to logarithmic weight gains. However, as seen from Fig. 5, the added nano-sized SiC particles were observed to decrease the starting oxidation temperature of Alon ceramic from 1000 °C to 700 °C. This was likely due to the fact that the nano-sized SiC particles had more cumulative surface area and higher total surface energy than the micro-sized Alon matrix (Fig. 1). Likewise, Kaur et al.[31] studied the oxidation behaviour of green coke-based carbon–ceramic

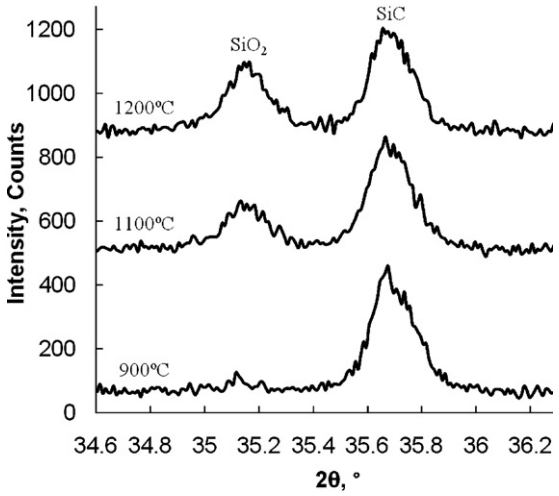

Fig. 10. XRD patterns obtained at a slower scan rate, showing the change of the (1 1 1) peak of SiO_2 and (0 0 6) peak of SiC in the 8 wt% SiC–Alon composites with the temperature of oxidation in air for 40 h.

composites incorporating micro- and nano-SiC particles, and reported that the weight gain was higher in the composites containing nano-SiC particles as compared to the composites containing micro-SiC particles. Similar results were also observed by Jia et al.[32] who reported that the starting temperature of oxidation was about 843 °C for 1.2 μm SiC particles, while it decreased to 783 °C for 0.2 μm SiC particles. In the present study, the size of added SiC particles was less than 0.1 μm (Figs. 1(b) and 4(b)), so that the starting temperature of oxidation was anticipated to be further lower, and the weight gain appeared at 700 °C (Fig. 5(b)). The weight gain of SiC–Alon composites in the oxidation tests starting from 700 °C (Fig. 5(b)) was attributed to the occurrence of SiO_2 via the following reaction,[25,33–35]

$$2SiC + 3O_2 \rightarrow 2SiO_2 + 2CO \uparrow . \quad (2)$$

This was confirmed by XRD results, as shown in Fig. 10. It should be pointed out that while the SiO_2 peak was clearly seen at 1100 °C and 1200 °C, it just started to appear at 800–900 °C. It was difficult to identify the SiO_2 peak at 700 °C due to the small amount of SiO_2 formed, which was believed to be below the detection limit of XRD even though it was scanned at a very slow rate. It was clear from Eq. (2) that the occurrence of oxidation from SiC to SiO_2 gave rise to an appreciable (49.89%) weight gain per reaction. If the oxidation of Alon and SiC would occur following Eqs. (1) and (2) concurrently, the weight gain in the oxidation of 8 wt% SiC–Alon composites would be estimated to be about 6.86% per reaction based on the following rule of mixtures,

$$\omega_c = \omega_m f_m + \omega_p f_p, \quad (3)$$

where ω_c is the weight change (gain or loss) per reaction in the composites (in %), ω_m is the weight change per reaction resulting from the oxidation of matrix (in %), ω_p is the weight change per reaction arising from the oxidation of reinforcement particles (in %), f_m is the weight fraction of matrix, and f_p is the weight fraction of reinforcement particles ($f_m = 1 - f_p$). Therefore, the weight gain per reaction in the oxidation of 8 wt%

SiC–Alon composites was more than twice that of pure Alon ceramic (3.12%) per reaction. That is, the oxidation of SiC–Alon composites was more sensitive to the weight gain due to the presence of nano-sized SiC particles (depending on the weight fraction or volume fraction of SiC particles). This would be another reason for us to detect more easily the weight gain of 8 wt% SiC–Alon composites at lower temperatures of 700 °C, as shown in Fig. 5(b).

Although the addition of nano-sized SiC particles decreased the starting oxidation temperature of Alon composites mainly stemming from the large cumulative surface area and high total surface energy as mentioned earlier, it can effectively improve the mechanical properties,[16,36] and remarkably enhance the oxidation resistance of SiC–Alon composites at higher temperatures of 1100 °C and 1200 °C, as shown in Fig. 5(b) (and also in Fig. 8(f) in comparison with the oxidation layer thickness of pure Alon at 1200 °C (Fig. 8(e)). This would be attributed to the essential contribution of the presence of SiO_2 and Al_2O_3. As seen from Fig. 6, the oxidation layer of SiC–Alon composites was generally denser than that of pure Alon. Similar to the conventional SiC ceramics and SiC whisker-reinforced ceramic composites, SiC particles especially those near the sample surface were susceptible to oxidation at temperatures above 1000 °C, forming SiO_2 which might subsequently react with the oxidation product Al_2O_3 of Alon matrix.[37] Therefore, a reacted scale was expected to form on the surface of the SiC–Alon composites during oxidation in air at high temperatures. As Wang et al.[30] pointed out, when the temperature was above 1200 °C, the addition of SiC was highly beneficial for improving the oxidation resistance of ZrB_2, as a result of the formation of a protective borosilicate glass layer. In the present study, the oxidation products in Fig. 6(f) were also expected to be the phase consisting of SiO_2 glass and aluminosilicate glass formed by the reaction of SiO_2 and Al_2O_3. These products can fill and bond the position of pores and cracks, leading to a dense oxidation surface layer. Such a dense layer can block the inward diffusion of oxygen through the oxidation layer (i.e., step 2 of oxidation as mentioned earlier), thus enhancing considerably the oxidation resistance or reducing the weight gain, as shown in Fig. 5(b). This was similar to the observations reported by Takahashi et al.,[38] where the SiC could heal the cracks and toughen Al_2O_3 materials when the temperature was above 1100 °C. Similar results were also reported in,[34,39,40] where the oxygen diffusion was observed to be much slower through the silica layer than through the matrix, and the oxidation was controlled by the inward diffusion through the Al_2O_3/SiO_2 layer. Hence, the combined action of Al_2O_3 and SiO_2 in the SiC–Alon composites resulted in the formation of a dense protective layer which reduced the rate of further oxidation (Fig. 5(b)), and led to a change of oxidation kinetics from the linear-like increase in the pure Alon ceramic (Fig. 5(a)) to a logarithmic-like increase of the weight gain in the SiC–Alon composites (Fig. 5(b)) which could be expressed as,

$$W = K_1 \log(K_2 t + K_3), \tag{4}$$

where K_1, K_2 and K_3 are constants (K_3 should be 1 if one considers zero weight gain at zero time).

Furthermore, the Pilling–Bedworth ratio (P–B ratio), R, might be used to estimate if an oxidation layer is protective. The P–B ratio, originally proposed for a metal oxide, which is produced by the reaction of metal and oxygen, is defined as the ratio of the volume of the metal oxide to the consumed metal volume,[41,42]

$$R = \frac{v_o}{v_M} = \frac{A_o \rho_M}{\alpha A_M \rho_o}, \tag{5}$$

where α is the coefficient of the metal species for the overall oxidation reaction, A_o is the molecular (or formula) weight of the oxide, A_M is the atomic weight of the metal, and ρ_o and ρ_M are the densities of oxide and metal, respectively. In the present case of ceramic materials, the Alon ($Al_{2.81}O_{3.56}N_{0.44}$) and SiC are assumed to be akin to the above metal matrix. Then the P–B ratios for the oxidation of Alon and SiC in terms of Eqs. (1) and (2) would be estimated to be about 0.96 and 1.82, respectively, based on the densities of 3.688 g/cm^3, 3.95 g/cm^3, 3.21 g/cm^3 and 2.65 g/cm^3 and the molecular weight of 138.93 g/mol, 101.96 g/mol, 40.10 g/mol and 60.09 g/mol for $Al_{2.81}O_{3.56}N_{0.44}$, Al_2O_3, SiC and SiO_2, respectively. It follows that the oxidation product of Al_2O_3 arising from Alon would not have any protective role since the Al_2O_3 oxide layer tended to be porous and was insufficient to fully cover the whole sample surface when R was less than unity.[41] This could basically be seen from the loose morphology in Fig. 6(a), (c) and (e), thus giving rise to an almost linear kinetic characteristic (Fig. 5(a)). On the contrary, an R value of 1.82 for the oxidation of SiC just laid in-between 1 and 2 within which the formed oxide layers were pointed out to be capable of covering the surface and provide proper protection to the further oxidation.[41] This could be seen from the dense surface morphology of SiC–Alon composites after oxidation at 1200 °C (Fig. 6(f)), leading to a progressively slower logarithmic kinetic feature, as shown in Fig. 5(b) and expressed by Eq. (4).

Finally, it should be noted that no mullite was formed in the SiC–Alon composites, since the mullite normally appeared at a temperature of above 1400 °C.[28] This was confirmed by XRD analysis (Fig. 9(b)) where the detected crystalline phases of oxidation products on the surface were just Al_2O_3 and SiO_2. Similar results at oxidation temperatures below 1400 °C were also reported by Baudin and Moya.[33] In a word, there is clear evidence that nano-sized SiC particle added to Alon ceramic resulted in an increase in the oxidation resistance at high temperatures up to 1200 °C. More studies are needed to understand the oxidation mechanisms of SiC–Alon composites at further higher temperatures at which the mullite phase could be formed.

5. Conclusions

In the present study, the oxidation characteristics of aluminium oxynitride (Alon) and nano-sized silicon carbide–aluminium oxynitride (SiC–Alon) composites with a relative density of 97% was investigated over a temperature range of 700–1200 °C in air. It was observed that the Alon matrix and SiC particles near the sample surface were oxidized to form Al_2O_3 and SiO_2, respectively. However, no mullite

phase was formed within this temperature range. The starting oxidation temperature of pure Alon ceramic was observed to be about 1000 °C below which no obvious oxidation was detected. The oxidation products appeared in the order of needle-like, flake-like and layer-like forms during the oxidation process at high temperatures. With the addition of nano-sized SiC particles, while the starting oxidation temperature was decreased to about 700 °C due to the large cumulative surface area and high total surface energy, the oxidation resistance at higher temperatures above 1100 °C was considerably enhanced. In particular, the oxidation kinetics changed from almost a linear weight gain as a function of time for the pure Alon to a logarithmic weight gain for the SiC–Alon composites. This was attributed to the formation of denser oxidation layers due to the presence of SiO_2 stemming from the added nano-sized SiC particles, which acted as a protective layer and suppressed the further penetration of oxygen, thereby effectively improved the high temperature oxidation resistance of the SiC–Alon composites. More studies are needed to identify the oxidation mechanisms of SiC–Alon composites at further higher temperatures where the mullite phase appeared.

Acknowledgments

The authors would like to thank the financial support of Natural Sciences and Engineering Research Council of Canada (NSERC) and National Natural Science Foundation of China (NSFC grant numbers 51072121 and 50672060) in the form of international research collaboration. D.L. Chen is also grateful for the financial support by the Premier's Research Excellence Award, NSERC-Discovery Accelerator Supplement (DAS) Award, Canada Foundation for Innovation, and Ryerson Research Chair program. The authors would also like to thank Professor X.D. Sun, X.Y. Yue and W. Wang (Northeastern University) for the helpful discussion and suggestion, and X.Y. Wang and H.M. Kan (Shenyang University), Q. Li, A. Machin, J. Amankrah and R. Churaman (Ryerson University) for their assistance in the experiments. X.J. Zhao, as an international exchange Ph.D. student, also gratefully acknowledges the financial support provided by China Scholarship Council.

References

1. Corbin ND. Aluminum oxynitride spinel: a review. *J Eur Ceram Soc* 1989;**5**:143–54.
2. Zhao XJ, Chen DL, Ru HQ, Zhang N. Zirconium nitride nano-particulate reinforced Alon composites: fabrication, mechanical properties and toughening mechanisms. *J Eur Ceram Soc* 2011;**31**:883–92.
3. Zheng J, Forslund B. Carbothermal synthesis of aluminium oxynitride (AlON) powder: influence of starting materials and synthesis parameters. *J Eur Ceram Soc* 1995;**15**:1087–100.
4. Wang XD, Li WC, Seetharaman S. Thermodynamic study and synthesis of γ-aluminium oxynitride. *Scand J Metall* 2002;**31**:1–6.
5. Yamashita H, Yamaguchi A. Oxidation of aluminum oxynitride–boron nitride (AlON–BN) composite prepared by reaction sintering. *J Ceram Soc Jpn* 2001;**109**:94–9.
6. Boch P, Glandus JC, Jarrige J, Lecompte JP, Mexmain J. Sintering, oxidation and mechanical properties of hot pressed aluminium nitride. *Ceram Int* 1982;**8**:34–40.
7. Goeuriot P, Goeuriot-Launay D, Thevenot F. Oxidation of an Al_2O_3–γAlON ceramic composite. *J Mater Sci* 1990;**25**:654–60.
8. Wang XD, Wang FM, Li WC. Synthesis, microstructures and properties of γ-aluminum oxynitride. *Mater Sci Eng A* 2003;**342**:245–50.
9. Wang XD, Sichen D, Li WC, Seetharaman S. Kinetic studies of the oxidation of γ-aluminum oxynitride. *Metall Mater Trans B* 2002;**33**: 201–7.
10. Zheng CW, Yang ZM, Zhang JS. The high-temperature oxidation behavior of reaction-bonded porous silicon carbide ceramics in dry oxygen. *J Am Ceram Soc* 2010;**93**:2062–7.
11. Lefort P, Ado G, Billy M. Oxidation behavior of transparent aluminum oxynitride. *J Phys (Orsay)* 1986;**47**:521–5.
12. Goursat P, Goeuriot P, Billy M. Contribution a l'etude du systeme Al/O/N I-reactive de l' oxynitrure d'aluminium γ. *Mater Chem* 1976;**1**:131–49.
13. Yamashita H, Yanmaquchi A. Preparation and properties of aluminum oxynitride (γ-AlON). *J Ceram Soc Jpn* 2001;**109**:310–4.
14. Zhang ZT, Wang XD, Li WC. Kinetic studies of oxidation of γ-AlON–TiN composites. *J Alloys Compd* 2005;**387**:74–81.
15. Yamashita H, Yamaguchi A. Preparation and properties of AlON–SiAlON composites. *J Ceram Soc Jpn* 2001;**109**:434–9.
16. Djenkal D, Goeuriot D, Thevenot F. SiC-reinforcement of an Al_2O_3–γAlON composite. *J Eur Ceram Soc* 2000;**20**:2585–90.
17. Mandal S, Sanyal AS, Dhargupta KK, Ghatak S. Gas pressure sintering of β SiC–γ-Alon composite in nitrogen/argon environment. *Ceram Int* 2001;**27**:473–9.
18. Hamidouche M, Bouaouadja N, Olagnon C, Fantozzi G. Thermal shock behavior of mullite ceramic. *Ceram Int* 2003;**29**:599–609.
19. Aksay IA, Dabbs DM, Sarikaya M. Mullite for structural, electronic and optical applications. *J Am Ceram Soc* 1991;**74**:2343–58.
20. Qi JQ, Zhou JC, Pang W, He JF, Su YY, Liao ZJ, et al. Study on the preparation of AlON powder by solid state reaction method. *Rare Metal Mater Eng* 2007;**36**:88–91.
21. Zhang ZT, Li WC, Bater SY. Manufacture and properties of AlON–TiN particlulate composites. *Mater Des* 2005;**26**:363–8.
22. Eivani AR, Valipour S, Ahmed H, Zhou J, Duszczyk J. Effect of the size distribution of nanoscale dispersed particles on the Zener drag pressure. *Metall Mater Trans A* 2011;**42A**:1109–16.
23. Holm EA, Foiles SM. How grain growth stops: a mechanism for grain-growth stagnation in pure materials. *Science* 2010;**328**:1138–41.
24. Guo S, Todd RI. Quantitation optical fluorescence microproble measurements of stresses around indentations in Al_2O_3 and Al_2O_3/SiC nanocomposites: the influence of depth resolution and specimen translucency. *Acta Mater* 2011;**59**:2637–47.
25. Osendi MI. Oxidation behavior of mullite–SiC composites. *J Mater Sci* 1990;**25**:3561–5.
26. Jacobson NS. Corrosion of silicon-based ceramics in combustion environments. *J Am Ceram Soc* 1993;**76**:3–28.
27. Pichor W, Janiec A. Thermal stability of expanded perlite modified by mullite. *Ceram Int* 2009;**35**:527–30.
28. Boch P, Giry JP. Preparation and properties of reaction-sintered mullite-ZrO_2 ceramics. *Mater Sci Eng* 1985;**71**:39–48.
29. Meng SH, Liu CP, Liu GQ, Bai GH, Xu CH, Xie WH. Thermal shock stress considering dynamical behavior for ultra high temperature ceramic. *Solid State Sci* 2010;**12**:818–21.
30. Wang Y, Liang J, Han WB, Zhang XH. Mechanical properties and thermal shock behavior of hot-pressed ZrB_2–SiC–AlN composites. *J Alloys Compd* 2009;**475**:762–5.
31. Kaur M, Kumar S, Sengupta PR. Oxidation behavior of green coke-based carbon–ceramic composites incorporating micro- and nano-silicon carbide. *J Mater Sci* 2009;**44**:2128–36.
32. Jia QL, Zhang HJ, Li SP, Jia XL. Effect of particle size on oxidation of silicon carbide powders. *Ceram Int* 2007;**33**:309–13.
33. Baudin C, Moya JS. Oxidation of mullite–zirconia–alumina–silicon carbide composites. *J Am Ceram Soc* 1990;**73**:1417–20.
34. Lin CC, Zangvil A, Ruh R. Modes of oxidation in SiC-reinforced mullite/ZrO_2 composites: oxidation vs depth behavior. *Acta Mater* 1999;**47**:1977–86.

35. Liu HY, Weisskopf KL, Hoffmann MJ, Petzow G. Oxidation behavior of SiC whisker reinforced mullite (-ZrO_2) composites. *J Eur Ceram Soc* 1989;**5**:123–33.
36. Zhao XJ, Zhang N, Ru HQ, Sun YZ, Guo ZK. Hot-pressing sintering behavior and properties of AlON/SiC composites. *Adv Mater Res* 2010;**105–106**:184–7.
37. Sakka Y, Bidinger DD, Aksay IA. Processing of silicon carbide–mullite–alumina nanocomposites. *J Am Ceram Soc* 1995;**78**:479–86.
38. Takahashi K, Yokouchi M, Lee SK, Ando K. Crack-healing behavior of Al_2O_3 toughened by SiC whiskers. *J Am Ceram Soc* 2003;**86**:2143–7.
39. Lavrenko VA, Desmaison J, Panasyuk AD, Desmaison-Brut M. Oxidation resistance of AlN–(TiB_2–$TiSi_2$) ceramics in air up to 1450 °C. *J Eur Ceram Soc* 2003;**23**:357–69.
40. Zhang FC, Luo HH, Roberts SG. Mechanical properties and microstructure of Al_2O_3/mullite composite. *J Mater Sci* 2007;**42**:6798–802.
41. Callister Jr WD, Rethwisch DG.*Materials Science and Engineering: An Introduction*. 8th edition New York: John Wiley & Sons, Inc.; 2010. pp. 703–707.
42. Zhang G. Improving IC yield with protective ceramics. *Semicond Int* 2000;**23**:217–8.